Title

Two-Dimensional Mapping of In-plane Residual Stress with Slitting

Journal

Experimental Mechanics, 58(1)

ISSN

0014-4851

Authors

Olson, MD

Hill, MR

Publication Date

2018

DOI

10.1007/s11340-017-0330-y

Two-dimensional Mapping of In-plane Residual Stress with Slitting

M.D. Olson and M.R. Hill*
Department of Mechanical and Aerospace Engineering, University of California, One Shields Avenue, Davis, CA 95616

Submitted to *Experimental Mechanics*, March 2016
Revised, and Accepted for publication, August 2017

ABSTRACT

This paper describes the use of slitting to form a two-dimensional spatial map of one component of residual stress in the plane of a two-dimensional body. Slitting is a residual stress measurement technique that incrementally cuts a thin slit along a plane across a body, while measuring strain at a remote location as a function of slit depth. Data reduction, based on elastic deformation, provides the residual stress component normal to the plane as a function of position along the slit depth. While a single slitting measurement provides residual stress along a single plane, the new work postulates that multiple measurements on adjacent planes can form a two-dimensional spatial map of residual stress. The paper uses numerical simulations to develop knowledge of two fundamental problems regarding two-dimensional mapping with slitting. The first fundamental problem is to estimate the quality of a slitting measurement, relative to the proximity of a given measurement plane to a free surface, whether that surface is the edge of the original part or a free surface created by a prior measurement. The second fundamental problem is to quantify the effects of a prior slitting measurement on a subsequent measurement, which is affected by the physical separation of the measurement planes. The results of the numerical simulations lead to a recommended measurement design for mapping residual stress. Finally, the numerical work and recommended measurement strategy are validated with physical experiments using thin aluminum slices containing residual stress induced by quenching. The physical experiments show that two-dimensional residual stress mapping with slitting, under good experimental conditions

* Corresponding author. Tel.: 530-754-6178; fax: 530-752-4158.
E-mail address: mrhill@ucdavis.edu

(simple specimen geometry and low modulus material), has precision on the order of 10 MPa. Additional validation measurements, performed with x-ray diffraction and ESPI hole drilling, are within 10 to 20 MPa of the results from slitting.

Keywords: Residual stress, measurement design, slitting, mapping, superposition

1. INTRODUCTION

The present work is directed at developing a method for determining the two-dimensional distribution of one in-plane component of residual stress in a thin part, that can be idealized as a two-dimensional body. There are a wide range of potential techniques for residual stress measurement, with some providing residual stress at a point (e.g., hole drilling or x-ray diffraction) and others providing a profile of stress along a line (e.g., slitting or deep hole drilling). The contour method, invented by Prime [1], is unique in that it provides a two-dimensional distribution of the residual stress component normal to a plane. An example contour measurement from our earlier work [2] is shown in Fig. 1, comprising the measurement of quenching stress in a long bar (Fig. 1a). The contour method determines the stress normal to a plane of interest, and in the earlier study found that the stress along the length of the long quenched bar, σ_{zz}, had a paraboloid distribution in x and y (Fig. 1b). The contour method results are useful because they illuminate spatial variations of the stress field that may not be recognizable with a point or line measurement, which can be very useful for failure assessment or process model validation. The present work describes a method to determine a two-dimensional residual stress distribution, in x and y, like that provided by the contour method, but where the part is thin (along z), and the stress component of interest lies in the plane of the thin part (i.e., either σ_{xx} or σ_{yy}). An example of such a part is a thin slice of material removed near the middle of the long bar of Fig. 1a.

A two-dimensional distribution, commonly called a “map”, of one or more residual stress components might be determined in a variety of ways. A map of the near surface stress could be built up

by performing a series of point stress measurements using x-ray diffraction or hole drilling. Neutron diffraction could be used in a similar way, but with that method's larger sampling volume providing a thickness-averaged, rather than near surface, measurement. Some interesting measurements of quenching residual stress in thick aluminum bars were made using two diffraction techniques [3]. Those measurements comprise a very basic map of stress along three orthogonal lines, and because the measurements were in large parts they demonstrate the significant time and care required to form a map using diffraction. In welded materials, residual stress maps can also be obtained with diffraction, but with additional difficulties arising from spatial variations of stress-free lattice spacing, texture, and chemistry found in welds [4,5].

A map of the in-plane stress could also be built up by performing a series of line stress measurements. Such a map might be constructed from a series of deep hole drilling measurements [6] in thick parts or a series of slitting measurements [7] in thin parts. Recently, a technique comparison of in-plane residual stress mapping using hole drilling, neutron diffraction, and slitting was performed in a thin slice taken from a dissimilar metal weld [8]. The stress maps from each measurement technique showed that all three methods are capable of mapping in-plane residual stress, with slitting having lower experimental complexity and providing the best precision.

When mapping with a mechanical stress release method like slitting, care is required in placing adjacent measurements. In determining a suitable placement for each measurement, one must assure that a prior measurement does not affect a subsequent measurement, or that an anticipated effect can be accounted for. Upshaw et al. suggested when hole drilling measurements are placed five hole diameters apart, they can be considered independent [9]. Currently, there are no suggestions in the literature for recommended measurement spacing for slitting or deep hole drilling. However, work regarding the

contour method [10] and slitting [11] has demonstrated the ability to explicitly correct for the effect of a prior measurement on a subsequent one, with good accuracy.

This work is directed to develop methods for mapping one in-plane residual stress component in a thin body using a series of slitting measurements, since slitting has excellent measurement precision [12] and utilizes readily available equipment [13]. To fix ideas, consider a single slitting method measurement in a rectangular, two-dimensional part having width W along the x direction and height t along the along the y direction. A typical slitting method measurement is performed at the mid-width ($x = W/2$), and determines $\sigma_{xx}(W/2, y)$ (i.e., the residual stress component normal to the mid-width plane, as a function of height). The measurement consists of cutting a thin slit along the height, from $y = 0$ to $y = t$, while measuring part deformation as a function of cut depth. Cutting is typically performed using wire electric discharge machining (EDM) and deformation is typically measured using metallic foil strain gages. Given measured deformation as a function of cut depth, residual stress is computed using an elastic inverse. A map of stress could be formed by making a number of slitting measurements on adjacent planes, but a study is required to determine a means to maintain the quality of the slitting measurements and to account for the interactions between adjacent measurements.

The most fundamental concerns for using slitting for stress mapping can be framed by considering two adjacent measurements made on a single part. Assuming elastic behavior dominates, which is fundamental to slitting and all mechanical stress release measurement techniques, superposition allows any number of adjacent measurements to be planned from knowledge gained by studying two adjacent measurements. Consider a first measurement along the dashed line in Fig. 2, with the slit cut from $y = 0$ to $y = t$ and deformation measured by a single strain gage at $y = t$. Past work suggests that the quality of this measurement will depend on the distance from the part free edge to the slit plane, s_1, because it affects the response of the strain gage to stress on the cut plane (further discussed below). A second

measurement location is indicated with the dotted line in Fig. 2, which is a distance s_2 from the prior measurement. The first measurement affects the second measurement in two ways. First, the quality of the measurement will be affected by s_2 in the same way the first measurement was affected by s_1 (the distance from the free edge) and second, s_2 will determine the degree to which stress released during the first measurement will change the stress measured during the second measurement.

One approach to mapping is to choose s_2 large enough that the first slitting measurement does not affect the second. For the configuration of Fig. 2, a rule of thumb suggests that spacing would need to be $s_2 \approx t$, so that the measurement resolution along x would be quite coarse. However, if multiple identical articles are available, measurements could be made in a series of articles with offset measurement locations, and the results combined to reveal the spatial map. Either option is unlikely to be of general utility. For parts with strong spatial stress gradients, or to minimize the number of identical articles needed, it would be desirable to use small measurement spacing.

The initial goals of this paper are to determine values of s_1 and s_2 that are likely to be useful in slitting mapping. The first goal is to determine the effect of s_1 (and also s_2) on measurement uncertainty. The second goal is to determine the effect of s_2 on stress release due to the first measurement at the location of the second measurement, including a determination of s_2 such that the first measurement has a negligible effect on the second measurement. Because the first two goals are attained with numerical modeling, a third goal is to provide experimental confirmation of the numerical work. The physical experiments use a series of thin slices removed from the quenched aluminum bar of Fig. 1a, and demonstrate the effects of various choices made in designing a mapping experiment.

2. METHODS

A useful summary of the theoretical background for slitting is given in [7], with key details summarized here to support an understanding of an uncertainty analysis that enables achieving the first

goal of this work. Considering the orientation of Fig. 2, the unknown residual stress perpendicular to the slit plane, as a function of position y, $\sigma_{xx}(y)$, is assumed to be a sum of known basis functions, $P_j(y)$, having a set of unknown amplitudes A_j

$$\sigma_{xx}(y) = \sum_{j=1}^{m} A_j P_j(y). \tag{1}$$

The strain that would occur at the strain gage, for a particular cut depth a_i, $\varepsilon_{xx}(a_i)$, is related to the unknown amplitudes through a *compliance matrix*, C_{ij}

$$\varepsilon_{xx}(a_i) = \sum_{j=1}^{m} C_{ij} A_j. \tag{2}$$

Each entry of the compliance matrix is the strain that would occur in a body having a slit of depth a_i, when the slit faces are loaded by a traction distribution $P_j(y)$. Given a specific strain gage size and location, the entries of the compliance matrix may be determined using elastic finite element modeling, as was described earlier [14].

The unknown amplitudes, A_j, are determined from measured strain versus slit depth data. Adopting matrix notation, Eq. (2) becomes

$$\boldsymbol{\varepsilon} = \boldsymbol{C}\boldsymbol{A} \tag{3}$$

where $\boldsymbol{\varepsilon}$ is a column vector of strain measured at each slit depth, $\boldsymbol{C}$ is the compliance matrix having rows and columns reflecting slit depth and basis functions, respectively, and $\boldsymbol{A}$ is a column vector of amplitudes (with the number of rows corresponding to the number of basis functions). The compliance matrix often has more rows than columns, so that Eq. (3) is solved in a least squares sense

$$\boldsymbol{A} = \boldsymbol{B}\boldsymbol{\varepsilon} \tag{4}$$

where $\boldsymbol{B}$ is the pseudoinverse [15] of $\boldsymbol{C}$

$$\boldsymbol{B} = (\boldsymbol{C}^T\boldsymbol{C})^{-1}\boldsymbol{C}^T. \tag{5}$$

An uncertainty estimate for residual stress measured by slitting was developed by Prime and Hill [16]. A column vector of stress variance (square of uncertainty), with rows reflecting stress at a series of discrete y values (usually taken to be the cut depths), is given by

$$\boldsymbol{s}^2 = diag(\boldsymbol{PB}[DIAG(\boldsymbol{u}^2{}_{\varepsilon})]\boldsymbol{B}^T\boldsymbol{P}^T) \tag{6}$$

where $\boldsymbol{u}^2{}_{\varepsilon}$ is a column vector of the strain variance with rows reflecting the cut depths, $\boldsymbol{P}$ is a matrix containing the values of $P_j(y_k)$, with rows corresponding to the discrete y values and the columns correspond to the basis functions, *diag* is an operator that forms a vector from the diagonal values of a matrix, and *DIAG* is an operator that forms a diagonal matrix from the values of a vector. Typically, the strain variance is either assumed constant at all depths, or computed as the difference between the measured strain and the strain fit, $\boldsymbol{u}_{\varepsilon} = \boldsymbol{\varepsilon} - \boldsymbol{CA}$.

There are two commonly used basis functions for slitting, Legendre polynomials and unit pulses. The Legendre polynomials were used historically [13], and are useful because they automatically satisfy mechanical equilibrium (taking only second and higher order terms of the series) and also reflect reasonable (plausible) residual stress fields, which makes them useful for measurement design. For example, the second order Legendre polynomial is similar to a residual stress field induced with quenching [17] and the sixth order Legendre polynomial is similar to a residual stress field induced with peening [18]. Unit pulse basis functions are newer and are very useful from an experimental perspective because they can resolve more general stress fields, including those with sharp stress gradients (e.g., as may arise from laser shock peening [19]). With unit pulse basis functions, supplementing the stress calculation procedure with Tikhonov regularization provides useful smoothing [20]. Both basis functions are used in this work. The Legendre polynomials are used for the numerical experiments and

the unit pulses are used in the physical experiments (to take advantage of the strengths of each basis function, as just described).

With an uncertainty estimate established, the effect of s_1 on measurement quality can be found by determining the uncertainty inherently associated with measurement for a range of values of s_1. This approach follows on the work of Rankin and Hill, who used the numerical quality of the compliance matrix, which correlates with stress uncertainty, as a basis for selecting strain gage configurations in slitting [21].

To understand how measurement uncertainty varies with s_1, a series of compliance matrices were developed with a range of values of s_1. The analysis considered a body with unit height, t, and width $W_1 = 3t$, as shown in Fig. 2. The distance from the edge of the sample to the cut plane, s_1, was varied from $0.05t$ to $1.5t$. Each compliance matrix was determined using a finite element model with 400 elements evenly spaced along the height, and element size increasing with distance from the cut plane, varying from $t/400$ at the cut plane to $t/40$ at the free edge. Each compliance matrix assumed Legendre polynomial basis functions, orders 2 through 6, and cut depths evenly spaced by $0.01t$. The *inherent* stress uncertainty for a given value of s_1 was then found using Eq. (6), assuming 1 με uncertainty at all cut depths. The inherent stress uncertainty provides an estimate of the minimum uncertainty that is driven by the geometry of the experimental conditions and ignores all sources of bias error, such as selection of appropriate number of basis functions (or amount of regularization) [22] that can strongly influence total uncertainty. Comparison of the inherent uncertainty for various values of s_1 versus position in the depth, and as a root mean square over all depths, enables an assessment of measurement quality.

The procedure to use slitting to form a map is very similar to the procedure used to make a single measurement. For the second measurement, the compliance matrix would be different, since the new

width, $W_2 = W_1 - s_1 \neq W_1$. However, for the special case when $s_2 = s_1$, and W_2 remains large enough (more than 1.25t), the compliance matrix for the second measurement can be assumed to be the same as the compliance matrix for the first measurement, since the first slitting measurement essentially creates a new free surface. If the measurements are close enough to one another, the effect of the first slitting measurement on the second should be accounted for, and would depend on s_2. For small values of s_2, there should be a large effect, and for large values of s_2, there should be a negligible effect.

The effect of a prior measurement on a subsequent one will be accounted for using a *correction*, which is determined using a supplemental stress analysis, similar to earlier work by Pagliaro, Prime et al. [10] and Wong and Hill [11]. Pagliaro et al. used a supplemental stress analysis to determine the effect of a prior contour method measurement on stress at a subsequent measurement plane, where the plane was orthogonal to and intersected the original measurement plane. Wong and Hill extended that idea to the slitting method, where two slitting measurements were made on orthogonal planes. In both of these earlier studies, the supplemental stress analysis used stress determined in the prior measurement as a traction boundary condition input in a stress analysis whose geometry reflected the configuration of the subsequent measurement (i.e., the analysis included the prior cut from contour or from slitting). The measured stress was applied as a traction on the prior cut plane, and stress was determined at the subsequent measurement plane. Here, the correction is used for two *parallel* measurement planes. The analysis is illustrated in Fig. 3, and used commercial finite element software [23]. The correction approach determines the stress originally present at the subsequently measurement plane as a sum of the output of the supplemental stress analysis at the subsequent plane and the stress that will be measured at the subsequent plane. This process is repeated for each subsequent measurement, where the supplemental stress analysis uses the total original stress present at the prior measurement plane. (An alternative, expedient supplemental stress analysis uses only the measured stress from each prior measurement as the applied traction, rather than total original stress, and extracts the stress from the

analysis at all subsequent measurement planes. This approach has the advantage that the corrections for all planes are computed in one step for each measurement.)

To determine the effect of s_2 on stress release due to the first measurement at the location of the second measurement, the second through sixth order Legendre polynomials (L_2 through L_6) were used to find how corrections for a set of plausible residual stress fields vary as function of s_2. The analyses applied a traction boundary condition to one edge of a model with a unit height, t, and a variable width, W_2. To understand how stress fields vary with part width, W_2 was varied from $0.25t$ to $2t$. The stresses caused by the polynomial tractions are extracted from the model at various values of s_2, $0 < s_2 < W_2$.

A series of physical experiments were performed to test the conclusions drawn from the numerical results, including both the effects of s_1 and s_2. Measurements were made on 5 mm thick slices removed from a long 7050 aluminum alloy bar that had been quenched to induce high residual stresses indicative of the T74 temper. The slices have a width of 77.8 mm and a height of 50.8 mm. The coordinate system used in this work has the origin at the center of the slice in the horizontal direction (38.9 mm from the edge) and at the bottom of the slice. The x-direction is positive to the right and the y-direction is positive up. All slitting measurements cut from $y = 0$ to 48.9 mm (to a depth 96% of the part height). A total of six slices were used in this work and will be called slice 1, slice 2, etc. The first four slices were used to form a map of stress in the slice. Slice 1 had measurements at -20 mm, 0, and 20 mm; slice 2 had measurements at -15 mm, 0, and 15 mm; slice 3 had measurements at -10 mm, 0, and 10 mm; and slice 4 had measurements at -5 mm, 0, and 5 mm, all of which can be seen in Fig. 4. The remaining two slices (slices 5 and 6) were used to test if the measurement order would affect the measured result. Slices 5 and 6 used the same measurement locations as slice 3, but altered the order so that the stress at each spatial location could be measured with a different measurement order. The measurement locations and cut

order can be seen in Table 1 and the choice of s (s_1, s_2, and s_3) for each measurement can be seen in Table 2.

The stress in each slice was measured on three planes of constant x. The stress at the third measurement plane is found using the same methodology as is used to calculate the stress at the second measurement plane, except that the traction boundary condition applied in the supplemental stress analysis is the total stress at the second measurement plane (i.e., the measured stress from slitting at the second measurement plus the correction from the first measurement at the second location).

The experiments followed best practices given by Prime [24] and by Hill [7]. Each measurement used a single strain gage mounted on the back face of the sample (y = 50.8 mm) with a 1.57 mm active gage length, and temperature compensated for aluminum. Each slitting measurement consisted of 60 cut increments, ranging in size from 0.25 to 1.5 mm. After each cut increment, the EDM wire was powered off and strain was recorded after allowing the Wheatstone bridge strain indicator to develop a stable readout (~1 min). Cut closure was avoided using visual inspection and cutting toward the initial cut depth as needed to maintain a gap on the cut plane. Elimination of cut closure is required given the linear formulation of Eq. (2). After the experiment, an instrumented optical microscope was used to determine the location of the slit, the location of the strain gage, the maximum slit depth, and the slit width.

A compliance matrix for each experiment was determined from a 2D, plane strain, finite element model and unit pulse basis functions for residual stress. The model reflected the measured geometry, which assures fidelity of measured residual stress [25], and assumed an elastic modulus of 70 GPa and Poisson's ratio of 0.3, to match aluminum. A typical model had 400,000 eight-node, biquadratic elements, with 1000 elements across the height and a bias of element size with distance away from the cut plane, with square elements at the cut plane and element size roughly 10x larger at the free end.

Lastly, since the compliance matrix is computed using a plane strain model, it was scaled using the correction scheme developed by Aydiner and Prime [26] to account for the finite thickness of the slice.

The uncertainty in each slitting measurement was calculated with Eq. (6). The strain uncertainty, u_ε, was taken as the maximum of either the difference between measured strain and strain fit, or a minimum value of 2 με. The uncertainty in the corrections for prior slitting measurements was estimated using a Monte Carlo approach. Each correction was found five times with a "noisy" stress distribution, where the noisy stress is the sum of the known, prior measured stress and noise corresponding to the uncertainty in the prior measurement. The error in the corrections was then taken as the standard deviation of the five corrections with added noise. The total uncertainty was found using

$$U = \sqrt{U_{slitting}^2 + U_{correction}^2} \tag{7}$$

where U is the total uncertainty of the stress in the slice, $U_{slitting}$ is the uncertainty from the slitting measurements, and $U_{correction}$ is the uncertainty in the prior measurement correction.

3. RESULTS

Fig. 5 shows that small values of s_1 result in large uncertainty in stress. The uncertainty as a function of cut depth, in Fig. 5a, has a similar distribution for different values of s_1, with uncertainty being largest at the initial cut depths and decreasing as cut depth increases. The similar shape of the uncertainty estimates is a result of the shape of the basis functions used in the stress calculation (i.e., $\boldsymbol{P}$ in Eq. (6)). The uncertainty is large for small values of $s_1 = 0.05t$ and $0.10t$, but quickly becomes smaller for $s_1 > 0.2t$. This is further illustrated in Fig. 5b, which shows the RMS of the uncertainty, across all cuts depths, as a function of s_1. The results show the uncertainty is significantly larger for small values of $s_1 = 0.05t$ and $0.10t$, but decreases rapidly and begins to plateau at $s_1 > 0.5t$.

Based on these results, we suggest the optimal selection of s (s_1, s_2, ... etc.) is $s = 0.2t$ as a balance between fine measurement spacing (small values of s) and reasonable measurement precision, since the uncertainty increases significantly for $s < 0.2t$.

The effect of s_2 on the stress release due to the first measurement at the location of the second measurement was assessed by applying Legendre polynomials as edge tractions to a set of models. A plot of the spatial variation of stress from the L_2 edge traction (Fig. 6a) shows that the stress is largest (and equal to the applied traction) at $x = 0$ and decays with increasing x to zero at the free surface of the far edge. Fig. 6b shows the stress plotted as a function of height at multiple lateral positions (i.e., values of s_2), which more clearly illustrates the variation of stress across the width of the sample. The maximum stress as a function of lateral position for various Legendre polynomial tractions is shown in Fig. 6c (normalized by the maximum applied traction), which shows that tractions with lower spatial frequency (like L_2) have further reaching effects than those with higher spatial frequency (e.g., L_6). A general residual stress profile can be thought of as a combination of several Legendre polynomials and since L_2 has the lowest spatial frequency it reflects a limiting case for additional analyses.

To further understand stress field variation relative to part width, the L_2 stress profile was applied to models with different widths. To reduce a two-dimensional stress field to one dimension, we plot the maximum value of the stress along y at a set of lateral positions representing potential planes for measurement, $x = s_2$, for parts with a range of widths, W_2. As shown in Fig. 7a, stress in parts with smaller values of W_2 become smaller more quickly, because no matter the choice of W_2, σ_{xx} will be zero at the opposite edge, which is a free surface. Fig. 7b shows that, on a relative scale, with x normalized by W_2, the stress in parts with smaller values of W_2 becomes smaller *relatively* more slowly along the part width.

A good mapping experiment would consist of having $s \geq 0.2t$. When this criterion is applied to the aluminum slices used in the present experimental work, we would expect good measurement precision for measurements with spacing of 20 mm ($0.39t$), 15 mm ($0.30t$), and 10 mm ($0.20t$), but poor measurement precision for the measurements with spacing of 5 mm ($0.098t$).

Measured strain data for all three measurements on slice 3 are given in Fig. 8a, and residual stresses are given in Fig. 8b. The strain and stress magnitudes are largest for the first measurement, which had $s_1 = 0.57t$, and are smaller and similar for the second and third measurements, which had $s_2 = s_3 = 0.2t$. It is expected that the strain signal would be the largest for the first measurement since there were no prior measurements. The corrections for the second and third measurement in slice 3 were very similar, as can be seen in Fig. 8c, which suggests that the initial stress was similar at the first and second measurement planes (since the correction at the second measurement is from the total stress at the first measurement location and the correction at the third measurement is from the total stress at the second measurement location). The total stress for the three measurements on slice 3, shown in Fig. 8d shows that the quenching induced stress is roughly parabolic along y, and relatively constant along x, over the 20 mm measurement span between planes 1 and 3 on slice 3.

The total stress at $x = 0$ in all six slices is shown in Fig. 9a. The measurements in slice 2, 3, 5, and 6 are nearly identical to one another, while the measurements in slices 1 and 4 differ somewhat. The measured stress for the first and third measurements (measurements at $x = \pm s$ from the mid-plane) in slices 1 through 4 can be seen in Fig. 9b. The measured stresses at ±20 mm are very similar to one another, showing symmetry that is expected in a part that was uniformly quenched. The same symmetry is evident in the results for measurements at ±15 mm, ±10 mm, and ±5 mm.

The results of the additional measurements intended to test the effects of measurement order using slices 3, 5, and 6 are shown in Fig. 10. The results show that although the individual slitting

measurements are different due to the order of the measurement, the total stress at the three different locations are nearly identical. Since the results are independent of measurement order, this confirms that superposition holds in the measurements, and that the measurements have good accuracy.

The two dimensional spatial maps of stress and uncertainty in Fig. 11 show tensile residual stress in the center of the slice, maximum near 60 MPa, and compressive stresses along the upper and lower edges, minimum near -100 MPa. (There are six measurements of stress at $x = 0$, but the results from slice 6 are used in the map because they are judged to have the best measurement fidelity.) The uncertainty map shows that the total uncertainty is very low (less than 8 MPa) for all measurements, except for the measurement at $x = 5$ mm. To better understand the how the uncertainty is affected by the choice of s, the RMS of the uncertainty for each slitting measurement, correction, and total have been plotted in Fig. 12 as a function of measurement spacing. Uncertainty due to the correction is smaller than the uncertainty due to slitting. As predicted, the results show the uncertainty increases significantly when the measurement spacing is 5 mm ($0.1t$). The uncertainties for the third measurements in slices 1 through 4 are shown as a function of position in Fig. 13 for both slitting and the corrections. The uncertainty for the slitting measurements increases with decreasing s, with the measurement with $s = 5$ mm having the largest uncertainties (15 MPa). The uncertainty in the corrections also has uncertainty increasing for decreasing s, with $s = 10$, 15, and 20 mm having small uncertainty (under 3 MPa), but $s = 5$ mm having a large uncertainty (30 MPa). For measurements with $s \geq 10$ mm, the uncertainties in the corrections are smaller than the uncertainties from slitting because the slitting uncertainties have high spatial frequency whose effect becomes small over a relatively short distance. The uncertainties in the experiments confirm what was determined in the numerical analysis, that using a small measurement spacing ($s = 0.1t$) leads to imprecise measurement.

4. DISCUSSION

The results presented above show several significant outcomes regarding mapping with slitting. A significant outcome is the experimental demonstration of slitting mapping, which provided good precision, except when the measurements were too closely spaced. The numerical analysis suggested, and experimental measurements confirmed, that measurement spacing of $s \geq 0.2t$ provides good measurement precision (around 5 MPa in the experiments on slice 3) while the spacing of $s = 0.1t$ results in poor precision (around 30 MPa in the experiments on slice 4). The numerical analysis shows that the poor precision for small values of s_1 (or s_2) is due to poor condition of the compliance matrix, because stress release does not cause strain change for shallow cut depths when s is small. This effect can be seen in Fig. 14, which plots the first column of the compliance matrix (strain for the L_2 traction) for a range of s. For a typical slitting configuration, such as $s = t$, there is some amount of strain change for all cut depths. When the slit is close to the edge of the coupon, such as for $s = 0.1t$ or $0.05t$, there is nearly zero strain change for shallow cut depths. Therefore, the poor performance of slitting with $s \leq 0.1t$ is expected, and experiments should use spacing of $s \geq 0.2t$.

The measured stresses at $x = 0$, in Fig. 9a, enable a comparison of measurement results for various choices of s and it is promising that the measurements in slice 2, 3, 5, and 6 show very good agreement. The measured strain and calculated stress for the second measurement on slice 4, with $s_2/t \approx 0.1$, is shown in Fig. 15, and clearly illustrates the poor outcome when measurement spacing is too small, with the measured stress being similar to the estimated uncertainty. It is therefore understandable that the second measurement in slice 4 results in an outlier in Fig. 9a. (It is confounding that the measurement in slice 1 does not agree well with the other results (by around 50 MPa at shallow cut depths and 10 MPa at the mid-height), especially since this measurement has low uncertainty (under 5 MPa).)

Typical slitting measurements use a back-face strain gage with the measurement plane at the specimen mid-width. The symmetry of that configuration makes the measurement invariant to shear stress on the measurement plane. For the slitting mapping approach developed here, shear stress effects are possible, and may lead to error. To assess potential for error from shear stress, we performed a further analysis.

Strain arising from shear stress release during slitting was computed using the same elastic stress analysis approach described above, and was compared to strain arising from normal stress release. The analysis was repeated for a characteristic shear stress distribution and a range of s_1/t values for $W_1/t = 4$. The distribution of shear stress used was a first-order modified Jacobian polynomial

$$J_1(y) = 8y/t(2y/t\text{-}1)(y/t\text{-}1) \tag{8}$$

which satisfies shear stress equilibrium (integrates to zero) and boundary conditions (zero at the free surfaces, $y = 0, t$) [27].

The strain that occurs for the J_1 shear stress is compared to strain for a L_2 normal stress in Fig. 16 for $s_1/t = 1$, 0.75, 0.4, and 0.2. The results show that the strain response is smaller for shear stress than for normal stress for all values of s_1/t and at all cut depths. For $s_1/t \geq 0.75$, the strain due to shear stress is very small relative to that from normal stresses, and might be considered negligible. However, for smaller values of s_1/t, the strain response from J_1 can be significant, especially for larger cut depths (Fig. 16a).

To estimate errors that could occur for unaccounted shear stresses, stresses were calculated using the strains for a normal stress of $100L_2$ alone, and combined with modified J_1 shear stresses of $20J_1$, $50J_1$, and $100J_1$. The stress calculations were as described above, and the calculations do not account for shear stress; therefore, the computed stress contains an error due to the strain caused by shear stress. Fig. 17

shows stress for $100L_2$ alone, and with added shear stress for a small value of s_1/t (0.2). When the magnitude of shear and normal stresses are equal, the error in the computed normal stress is significant (17% peak error), and smaller when the shear stress is smaller. For larger values of s_1/t, the effects of shear stress cause smaller errors. When $s_1/t > 0.5$, error from equal magnitude shear stress is less than 5%, and when $s_1/t > 0.75$, error from equal magnitude shear stress is less than 2.8%.

Due to the errors that are possible with significant shear stresses and small values of s_1/t, we suggest forming the slitting map by repeatedly bisecting the specimen at $W/2$ when $W/t \leq 1.5$. Cutting at $W/2$ and using a central, back-face strain gage is a symmetric configuration, so the measurement is insensitive to shear stress, and no error results.

The data found in the two fundamental numerical problems (as is shown in Fig. 5 through Fig. 7) have been distilled to produce Fig. 18, which can be used as an aid in the design of a mapping experiment. When designing the mapping experiment, the first item to consider is the limiting measurement spacing for large experimental uncertainty. The limits for good measurement precision are shown as dashed lines in Fig. 18, where the horizontal dashed line at $s/t = 0.2$ gives the minimum distance from the previous cut plane (or free edge) and the steepest inclined dashed line along $s/t = W/t - 0.2$ gives the minimum distance from the far edge of the coupon. The next item of interest in experiment design is the amount of stress remaining at a chosen measurement spacing, relative to the stress present prior to the first measurement (i.e., the original stress distribution). This can be found using the data in Fig. 7a, assuming the stress does not vary along the width of the bar and varies as L_2 along the height. The stress remaining at a given plane (for a given specimen width) is calculated by subtracting $\sigma_{max}/\sigma_{max(x=0)}$ in Fig. 7a from 1, since data in the figure provide the stress released by the prior measurement. Contours of remaining stress have been plotted in Fig. 18 for levels of remaining stress equal to 99%, 95%, 90%, 75%, 50%, 30%, and 10% of the original peak stress, as functions of s/t

and W/t. The results show a plateau behavior with increasing part width, where, for example, a part with $W_2 > 1.25t$, the stress will be 95% of the original peak stress if s is $0.74t$ (or larger). Smaller parts and smaller spacing result in more stress release, where, for example, a part with $W_2 = 0.75t$ measured at $s = 0.2t$ will have only 30% of the original stress. Because the figure is based on analysis for the L_2 stress profile, which is a limiting case, an arbitrary residual stress profile would exhibit less stress release than predicted using Fig. 18.

The s/t and W/t ratios used for the second ($x = 0$) and third measurements ($x = 10$ mm) in slice 3 were added to Fig. 18 to further illustrate the use of that chart, where the values for s_2, s_3, W_2, and W_3 are given in Table 2. Both measurements are on the boundary for good uncertainty (because they have $s/t \approx 0.2$), so we would expect good measurement uncertainty for both measurements (and that was confirmed in the measured results). The relative amount of stress remaining at each slitting location will also be explored. The relative amount of stress is computed as the peak magnitude for a given slitting measurement divided by the peak magnitude of the total stress at that plane. The relevant values of peak stress for the slitting measurements at $x = 0$ and 10 mm are 33 MPa and 32 MPa (Fig. 8b) and the values of total peak stress at $x = 0$ and 10 mm are 110 MPa and 92 MPa (Fig. 8d). The relative stress remaining at $x = 0$ is 30% (33 MPa / 110 MPa). To compare with the predicted relative amount of stress remaining at $x = 0$, $s_2/t = 0.197$ and $W_2/t = 0.96$ were added to Fig. 18, as shown by the square marker, which gives a remaining stress estimate of 30% that agrees with the measured ratio. Similar results are found at $x = 10$ mm, as the measured relative stress remaining is 35% (32 MPa / 92 MPa) and the estimated remaining stress is 30% (for $s_3/t = 0.197$ and $W_3/t = 0.77$), as shown by the star marker. Similarly, data for the third measurement in slice 1 ($x = 20$ mm, $s_3/t = 0.394$, $W_3/t = 0.77$), shown by the pentagon marker, and the second measurement in slice 2 ($x = 0$ mm, $s_2/t = 0.295$, $W_2/t = 1.06$), shown by the cross marker are included in Fig. 18. The estimated remaining stress for these two measurements, taken from Fig. 18, are 70% and 50% respectively. The measured remaining stress values are 71% (54.3 MPa /

76.9 MPa) and 49% (43.5 MPa / 89.2 MPa) for the measurements in slice 1 and slice 2, respectively. The excellent agreement between measured and estimated remaining stress derives from the similarity of the stress field in the physical experiments and that assumed in the analysis, which is evident in the weak dependence (assumed independent) of stress with x for the three measurements (Fig. 8d) and the similarity of the stress profile along y to L_2 (Fig. 8d). The present results provide confidence in the results of the numerical experiments, and illustrate the usefulness of Fig. 18 for measurement design.

The results of the numerical studies could be used to redesign the experimental slitting map using two extreme cases that may be of interest. One is the case when the measurements are spaced far enough apart that there is a negligible effect of a prior measurement on a subsequent one. This case has the advantage of having good precision while not requiring additional stress analysis (corrections). But, the large measurement spacing comes at the cost of requiring more material than would be needed if the measurements were more closely spaced. The other extreme case is when the measurements are as close as possible, while having reasonable measurement precision. This case uses a minimum of material, but has the burden of additional stress analyses required for correcting subsequent measurements for the effect of prior measurements, moderately larger uncertainty, and possibly larger errors if significant shear stresses are present.

The redesign of the previous experimental work using these two extreme cases assumes the objective is to map stress over the interval -25 mm $\leq$ x $\leq$ 25 mm, with a measurement pitch of 5 mm. For either approach, multiple slices are required, and measurement spacing can be determined with that aid of Fig. 18. First, we plan the experiment that requires no correction for prior measurements. The first measurement is placed at the boundary of the measurement area, x = -25 mm (s_1 = 13.9 mm). Following the first measurement, the remaining part has a width W_2 = 63.9 mm, or W_2/t = 1.26. Assuming 95% of the original peak stress remaining is sufficient (or, 5% stress release), we enter Fig. 18 with W_2/t = 1.26

and read over to $s_2/t \approx 0.75$ or $s_2 = 38.1$ mm, so that the second measurement would be placed 40 mm from the first measurement, at $x = 15$ mm. To determine the location of a third measurement, we repeat the same procedure. The relevant parameters are $W_3 = W_2 - s_2 = 26.3$ mm, or $W_3/t = 0.52$, and from Fig. 18, at 95% stress of original stress, we find $s_3/t = 0.43$, or $s_3 = 21.8$ mm, so that the third measurement, at $x \approx 37$ mm, would fall outside the measurement area. Therefore, only two measurements could be made on each slice, spaced 40 mm apart. The measurement design is shown in Fig. 19a, with two measurements made on each of three slices, and then single measurements on an additional five slices. The map requires a total of eleven measurements, made in eight slices.

Redesigning the experiment to use the minimum amount of material, we set the measurement spacing to be $0.2t \approx 10$ mm. The measurement design is shown in Fig. 19b, and requires only two slices, with 6 measurements in one slice and 5 measurements in the other. The amount of material required to develop the stress map is significantly reduced. With this plan, the amount of stress released by prior measurements is significant for each subsequent measurement. Considering measurements on the first slice, the stress remaining at the second measurement plane is only 30% of the original using Fig. 18 with $s_2 = 0.2t$ and $W_2 = 1.26t$. The stress remaining will be smaller than 30% for additional measurement planes since some amount of stress is released at all measurement planes from each prior measurement.

To further explore the fidelity of the two-dimensional stress map made with slitting, confirmatory residual stress measurements were made at the mid-height ($y = 25.4$ mm) of a slice as a function of x using EPSI hole drilling and x-ray diffraction. Both measurements followed standard practice, as described in [28] for ESPI hole drilling and [29] for x-ray diffraction. The measured results from the various techniques can be seen in Fig. 20, where ESPI hole drilling results are consistently higher than the slitting results, by around 10 MPa, and x-ray diffraction results are consistently lower than the slitting results, by 10 to 20 MPa. All three sets of results show a good degree of symmetry, which is

expected given the uniform quenching. Considering that 10 MPa is similar to the precision typical of any of the three measurement techniques [2], we judge all the results to be in good agreement.

A recently developed superposition based measurement approach that maps multiple residual stress components [30] requires the ability to map in-plane residual stress in a thin slice. The current work supports the use of slitting for the required in-plane stress map, and shows that it can provide a sufficiently refined spatial map with good measurement precision.

5. SUMMARY

The use of slitting to form a two-dimensional map of one in-plane residual stress component in a two-dimensional body has been considered in detail. Two numerical studies were performed to assess fundamental aspects of using slitting to form a map. The first numerical study assessed the fidelity of a slitting measurement as the distance to the part free edge is varied. The results of this numerical study show there would be very large uncertainties when the slitting measurement plane is close to either the part edge or a previous slitting measurement plane, and leads to a recommended minimum measurement spacing of $0.2t$. The second numerical study determined the effect of s_2 on stress release due to the first measurement at the location of the second measurement and showed stress release in parts with smaller values of W_2 become smaller more quickly; whereas on a relative scale, the stress release in parts with smaller values of W_2 become smaller *relatively* more slowly along the part width. The effects of shear stress release were investigated and showed the optimal approach for mapping is to repeatedly bisect the sample at $W/2$ when $W/t \leq 1.5$.

Two extreme cases of slitting mapping have been described. One case has the measurements far apart, so that the effects of prior measurements on subsequent measurements are negligible. This case requires eight slices to form the hypothetical stress map. The other extreme case minimizes the amount of material needed, and requires two slices to form the hypothetical stress map.

The results of both numerical studies were confirmed with physical experiments using slices that had residual stresses induced by quenching. The physical experiments, which had a specimen with simple geometry and low modulus material, showed excellent precision (under 10 MPa) for measurements with spacing greater than 0.2*t*. Results from confirmatory measurements made with x-ray diffraction and ESPI hole drilling agree well with the slitting mapping results, giving further confidence in the use of slitting to form a two-dimensional map of in-plane stress.

6. ACKNOWLEDGEMENTS

The authors acknowledge financial support from the Electric Power Research Institute, Materials Reliability Program (Paul Crooker, Senior Technical Leader), and technical support from Daniel Goldin and Kyler Steele (undergraduate student researchers at UC Davis). Special thanks to Professor Jeremy Robinson (University of Limerick) for the x-ray diffraction measurements and Adrian DeWald (Hill Engineering, LLC) for the EPSI hole drilling results presented in this paper.

REFERENCES

[1] M. B. Prime, "Cross-Sectional Mapping of Residual Stresses by Measuring the Surface Contour after a Cut," *Journal of Engineering Materials and Technology,* vol. 123, pp. 162-168, 2001.

[2] M. R. Hill and M. D. Olson, "Repeatability of the Contour Method for Residual Stress Measurement", *Experimental Mechanics,* vol. 54, pp. 1269-1277, 2014.

[3] J. S. Robinson, D. A. Tanner, S. van Petegem, and A. Evans, "Influence of Quenching and Aging on Residual Stress in Al–Zn–Mg–Cu alloy 7449," *Materials Science and Technology,* vol. 28, pp. 420-430, 2012.

[4] C. Ohms, R. C. Wimpory, D. E. Katsareas, and A. G. Youtsos, "NET TG1: Residual Stress Assessment by Neutron Diffraction and Finite Element Modeling on a Single Bead Weld on a Steel Plate," *International Journal of Pressure Vessels and Piping,* vol. 86, pp. 63-72, 2009.

[5] P. J. Bouchard, "The NeT Bead-on-plate Benchmark for Weld Residual Stress Simulation," International Journal of Pressure Vessels and Piping, vol. 86, pp. 31-42, 2009.

[6] D. J. Smith, "Deep Hole Drilling", in *Practical Residual Stress Measurement Methods*, Ch. 3, pp 65-87, John Wiley & Sons, West Sussex, UK, 2013.

[7] M. R. Hill, "The Slitting Method", in *Practical Residual Stress Measurement Methods*, Ch. 4, pp 89-108, John Wiley & Sons, West Sussex, UK, 2013.

[8] M. D. Olson, M. R. Hill, B. Clausen, M. Steinzig, and T. M. Holden, "Residual Stress Measurements in Dissimilar Weld Metal", *Experimental Mechanics,* vol. 55, pp. 1093-1103, 2015

[9] D. Upshaw, M. Steinzig, and J. Rasty, "Influence of Drilling Parameters on the Accuracy of Hole-Drilling Residual Stress Measurements," in Engineering Applications of Residual Stress, Volume 8, 2011, pp. 95-109.

[10] P. Pagliaro, M. B. Prime, H. Swenson, and B. Zuccarello, "Measuring Multiple Residual Stress Components using the Contour Method and Multiple Cuts", *Experimental Mechanics,* vol. 50(2), pp. 187-294, 2010.

[11] W. Wong and M. R. Hill, "Superposition and Destructive Residual Stress Measurements", *Experimental Mechanics,* vol. 53, pp. 339-344, 2013.

[12] M. J. Lee and M. R. Hill, "Intralaboratory Repeatability of Residual Stress Determined by the Slitting Method," *Experimental Mechanics,* vol. 47, pp. 745-752, 2007.

[13] M. B. Prime, "Residual stress measurement by successive extension of a slot: The crack compliance method," *Applied Mechanics Review,* vol. 52, pp. 75-96, 1999.

[14] M. J. Lee and M. R. Hill, "Effect of Strain Gage Length When Determining Residual Stress by Slitting", *Journal of Engineering Materials and Technology,* vol. 129, pp. 143-150, 2007.

[15] A. Albert, "Regression and the Moore-Penrose Pseudoinverse", Elsevier, New York, 1972.

[16] M. B. Prime and M. R. Hill, "Uncertainty, Model Error, and Order Selection for Series-Expanded, Residual-Stress Inverse Solutions," *Journal of Engineering Materials and Technology,* vol. 128, p. 175, 2006.

[17] M. B. Prime, M. A. Newborn, and J. A. Balog, "Quenching and Cold-work Residual Stresses in Aluminum Hand Forgings: Contour Method Measurement and FEM Prediction", in *Materials Science Forum*, pp. 435-440, 2003.

[18] M. R. Hill, A. T. Dewald, J. E. Rankin, and M. J. Lee, "Measurement of Laser Peening Residual Stresses", *Materials Science and Technology,* vol. 21, pp. 3-9, 2005.

[19] M. R. Hill and J. E. VanDalen, "Evaluation of Residual Stress Corrections to Fracture Toughness Values", *J ASTM Int,* vol. 5, pp 1-11, 2008.

[20] G. S. Schajer and M. B. Prime, "Use of Inverse Solutions for Residual Stress Measurement," *Journal of Engineering Materials and Technology,* vol. 128, pp. 375-382, 2006.

[21] J. E. Rankin and M. R. Hill, "Measurement of Thickness-average Residual Stress Near the Edge of a Thin Laser Peened Strip," *Journal of engineering materials and technology,* vol. 125, pp. 283-293, 2003.

[22] W. Cheng and I. Finnie, “Measurement of Through-Thickness Residual Stress” in *Residual Stress Measurement and the Slitting Method,* Ch. 7, pp 103-116, Springer Science + Business Media, LLC., New York, NY, USA, 2007.

[23] Abaqus/Standard, Version 6.10, Providence, RI, USA, 2010.

[24] M. B. Prime, "Experimental Procedure for Crack Compliance (Slitting) Measurements of Residual Stress," *Los Alamos National Laborary Report (LA-UR-03-8629),* 2003.

[25] M. R. Hill and W. Y. Lin, "Residual Stress Measurement in a Ceramic-Metallic Graded Material", *Journal of Engineering Materials and Technology,* vol. 124, p. 185, 2002.

[26] C. C. Aydıner and M. B. Prime, "Three-dimensional Constraint Effects on the Slitting Method for Measuring Residual Stress," *Journal of Engineering Materials and Technology*, vol. 135, 2013.

[27] W. Cheng and I. Finnie, “Residual Shear Stresses and K II Computation,” in *Fracture of Nano and Engineering Materials and Structures*, E. E. Gdoutos, Ed. Springer Netherlands, 2006, pp. 423–424.

[28] M. Steinzig and E. Ponslet, "Residual Stress Measurement using the Hole Drilling Method and Laser Speckle Interferometry: Part I", *Experimental Techniques,* pp. 43-46, 2003.

[29] J. S. Robinson, D. A. Tanner, C. E. Truman, A. M. Paradowska, and R. C. Wimpory, "The Influence of Quench Sensitivity on Residual Stresses in the Aluminium Alloys 7010 and 7075", *Materials Characterization,* vol. 65, pp. 73-85, 2012.

[30] M. D. Olson and M. R. Hill, "A New Mechanical Method for Biaxial Residual Stress Mapping", *Experimental Mechanics,* vol. 55, pp. 1139-1150, 2015.

TABLES

	x-position with corresponding cut order (mm)								
Slice	-20	-15	-10	-5	0	5	10	15	20
1	1				2				3
2		1			2			3	
3			1		2		3		
4				1	2	3			
5			1		3		2		
6			3		1		2		

Table 1: Measurement order and measurement plane locations for all slices

Slice	s_1 (mm)	s_2, s_3 (mm)	s_1/t	s_2/t, s_3/t	W_2/t	W_3/t
1	18.9	20	0.372	0.394	1.16	0.77
2	23.9	15	0.470	0.295	1.06	0.77
3	28.9	10	0.569	0.197	0.96	0.77
4	33.9	5	0.667	0.098	0.86	0.77
5	28.9	10	0.569	0.197	0.96	0.39
6	38.9	10	0.766	0.197	0.77	0.77

Table 2: Distances between measurement planes, *s*, normalized distances between measurement planes, *s*/*t*, and normalized widths, *W*/*t*

FIGURES

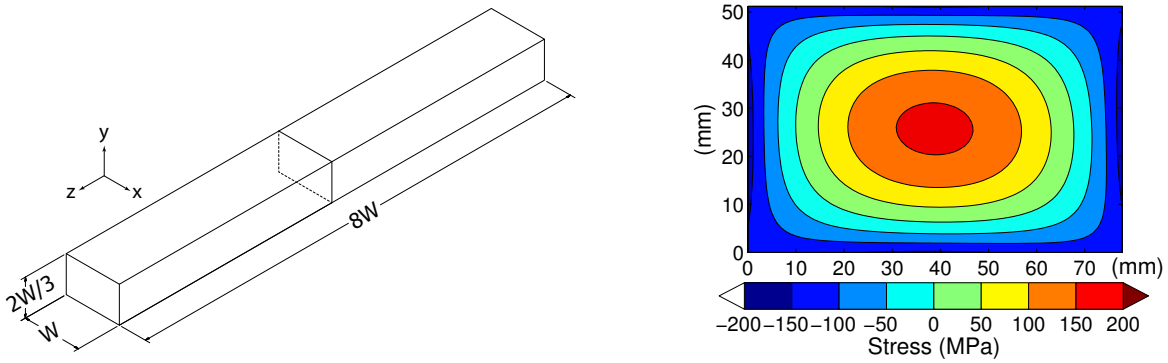

(a) (b)

Fig. 1 – (a) Diagram of a long quenched bar with a contour measurement plane at the mid-length (W = 77.8 mm) and (b) residual stress from a contour method measurement

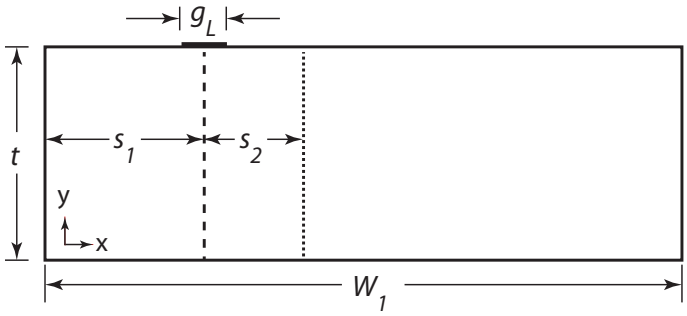

Fig. 2 – Geometry for the numerical study: t is the part height, W_1 the part width, g_L is the gage length, and s_1 is the distance from the edge to the gage center, and s_2 is the distance from the first to second measurement plane

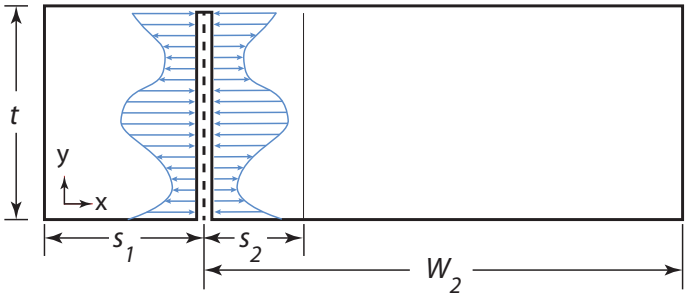

Fig. 3 – Geometry of the supplemental stress analysis used to find the correction for prior measurement: a traction boundary condition is applied to the cut faces of the prior measurement at $x = s_1$, and the resulting stress is extracted at the subsequent measurement plane, which is a distance s_2 from the prior measurement

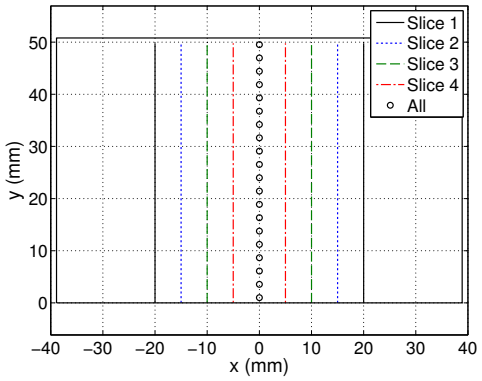

Fig. 4 – Diagram of the slitting locations

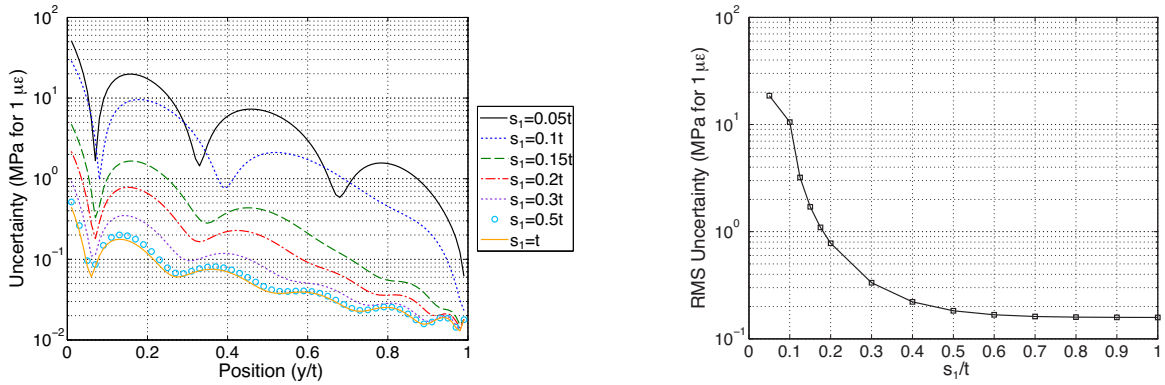

(a) (b)

Fig. 5 – Uncertainty in stress for 1 με strain error as a function of location of slitting plane from the edge of the coupon (s_1), (a) as a function of position (y/t) for various values of s_1/t, and (b) RMS uncertainty as a function of s_1/t

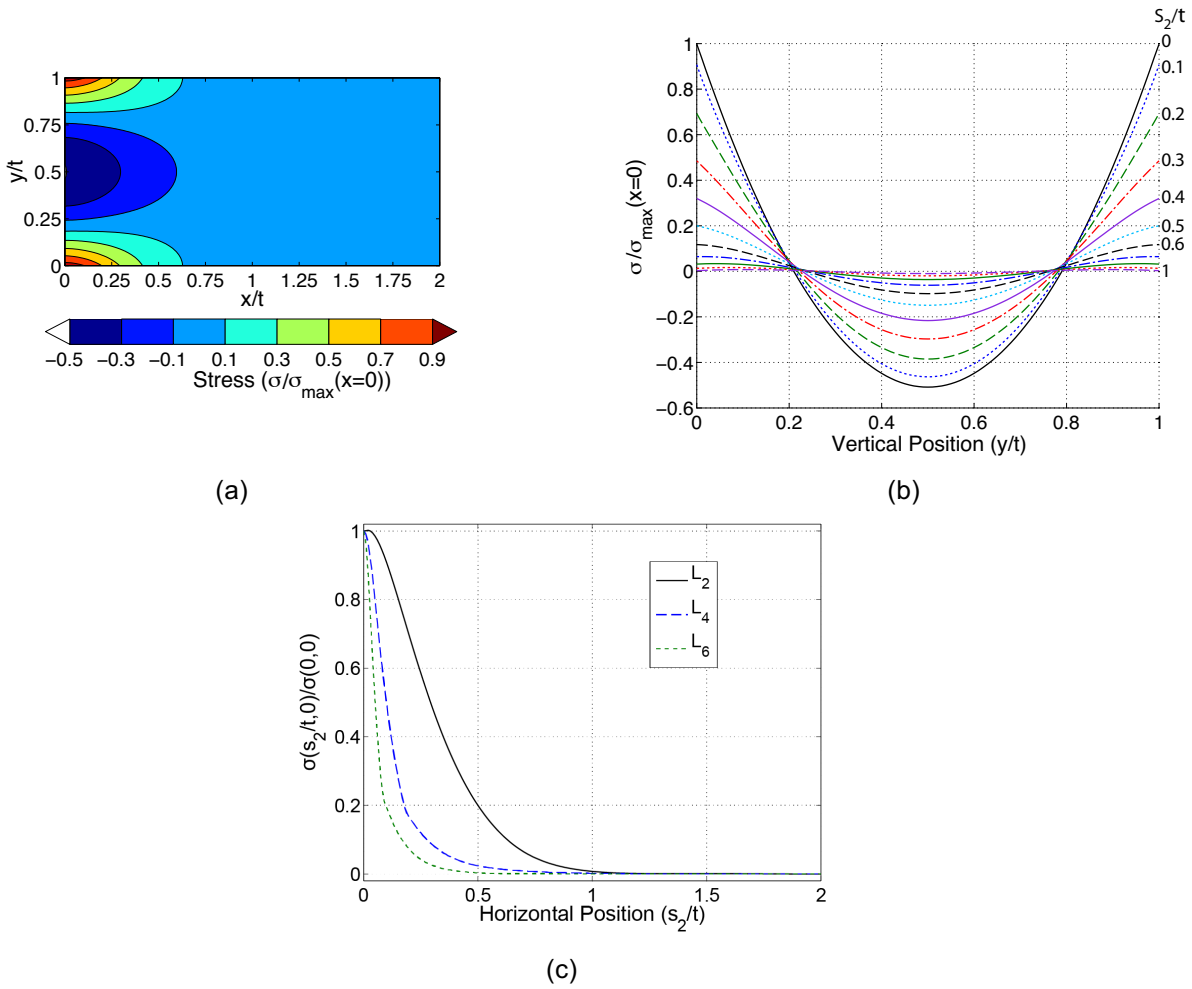

Fig. 6 – Stress as a function of position with an applied Legendre polynomial edge traction. (a) Contour plot of the spatial stress variation resulting from an applied L_2 edge traction, (b) line plot of the stress variation along the sample height for an applied L_2 edge traction, where $s_2/t = 0$ is the solid black line, $s_2/t = 0.1$ is the dotted blue line, and the others follow a trend of decreasing magnitude with increasing s_2/t, and (c) line plot of the maximum normalized stress (along the height) as function of s_2/t for the L_2, L_4, and L_6 Legendre polynomial edge tractions

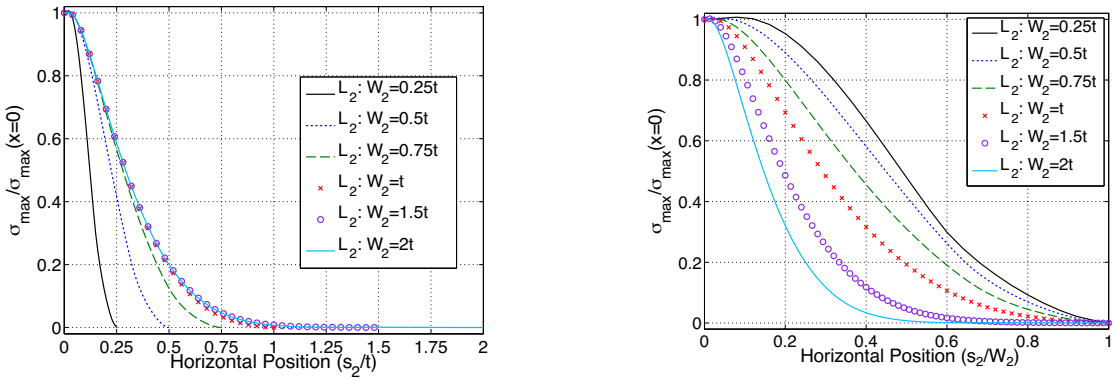

(a) (b)

Fig. 7 – Plot of the stress variation when applying an L_2 edge traction at $x = 0$ with variable sample width, W_2, (a) as a function of distance away from the cut plane (s_2/t) and (b) as a function of relative distance away from the cut plane (s_2/W_2)

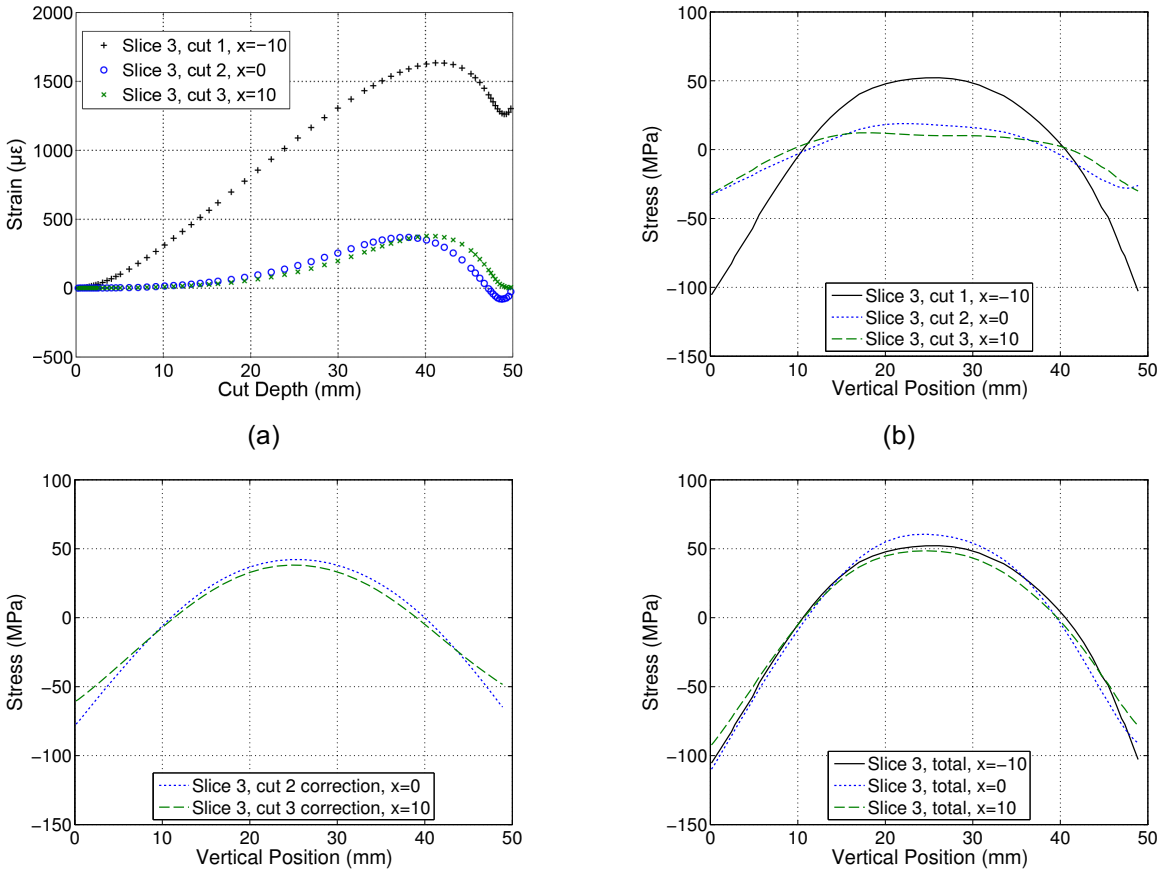

(a) (b)

(c) (d)

Fig. 8 – Line plots from slice 3 (10 mm measurement spacing) of the (a) measured strain, (b) computed stress, (c) corrections, and (d) total stress

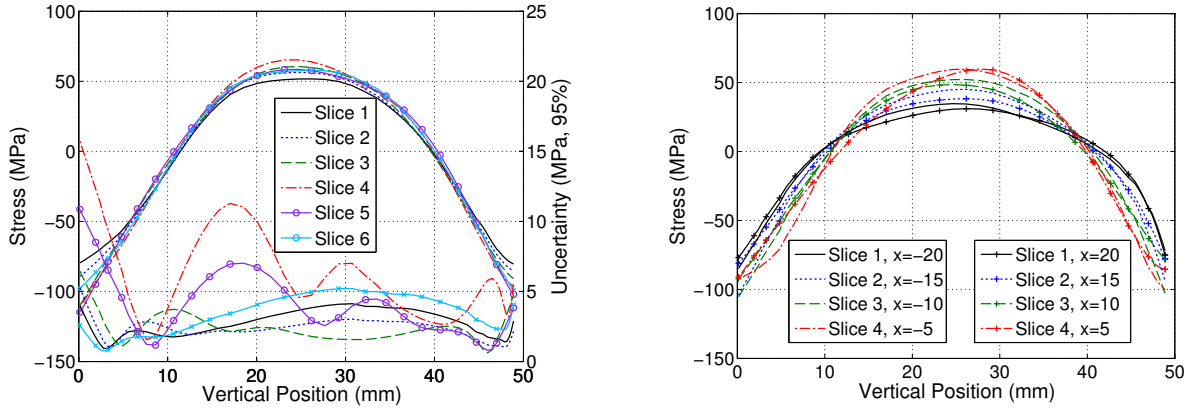

Fig. 9 – (a) The total stress at x = 0 mm and uncertainty (95% confidence interval, lines toward bottom of chart) and (b) the total stress at various positions symmetric about x = 0

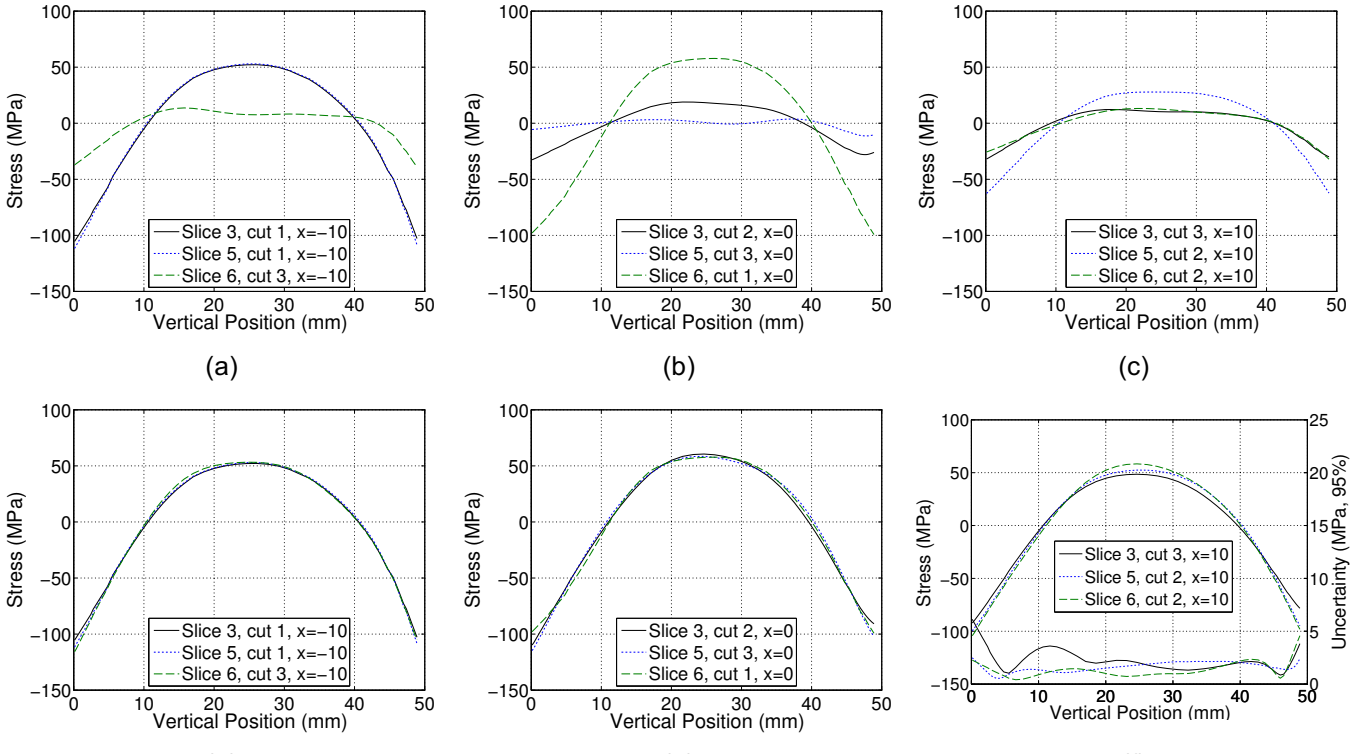

Fig. 10 – The measured slitting results from slices 3, 5, and 6 at (a) x = -10 mm, (b) x = 0, (c) x = 10 mm, and the total stress at (d) x = -10 mm, (e) x = 0, (f) x = 10 mm

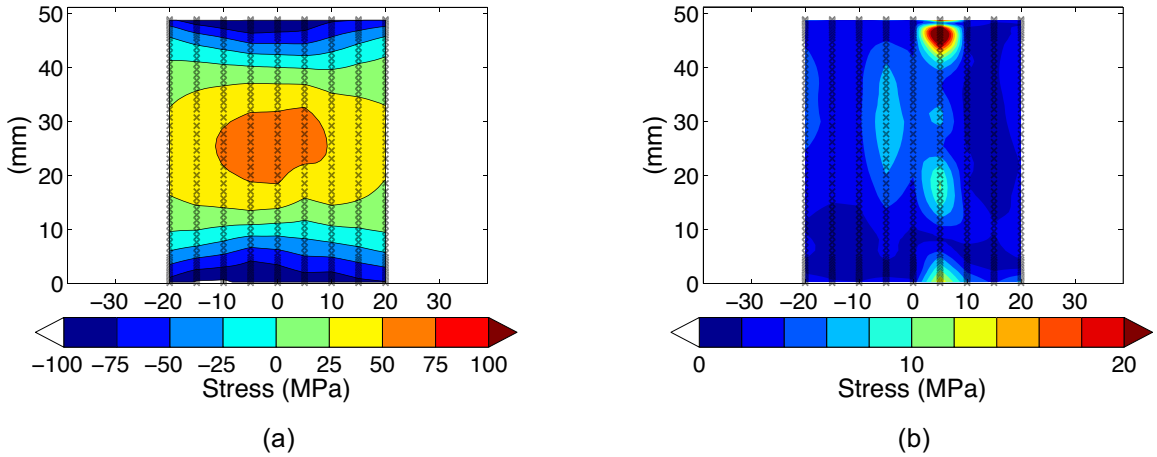

Fig. 11 – Maps of the total x direction (a) stress and (b) uncertainty

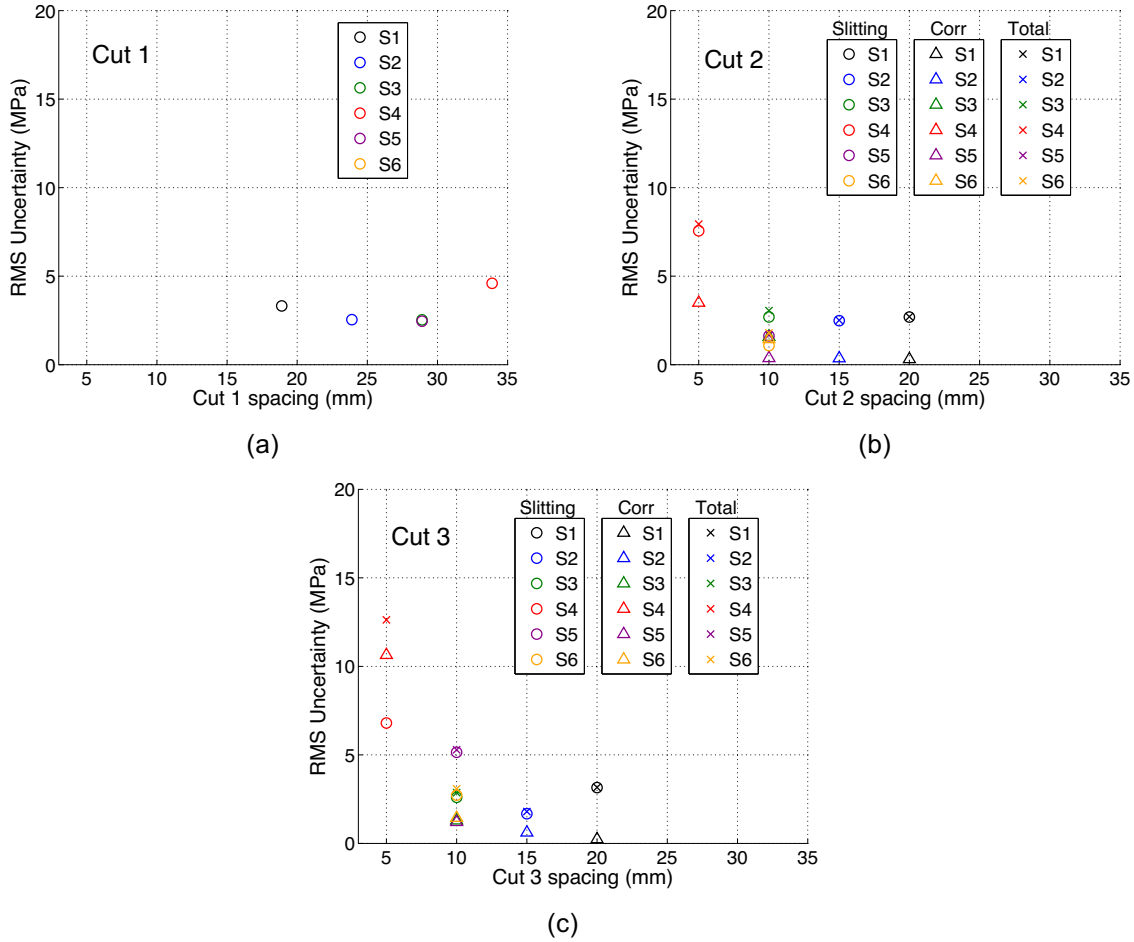

Fig. 12 – RMS uncertainty as a function of cut spacing for (a) cut 1, (b) cut 2, and (c) cut 3. Note: for cut 1 there is no correction, thus the total uncertainty is the same as the uncertainty from slitting

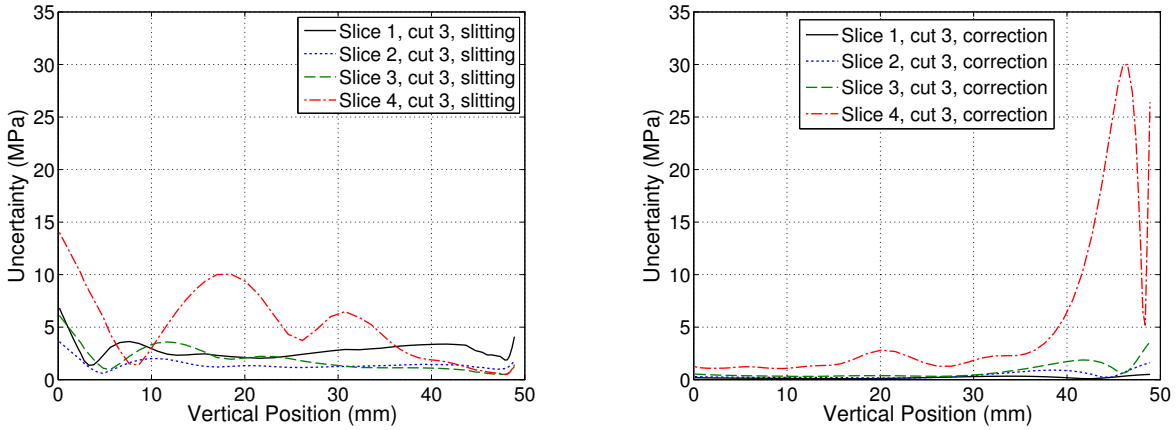

Fig. 13 – Line plots of the uncertainty (95% confidence interval) for the third measurement from (a) slitting and (b) corrections

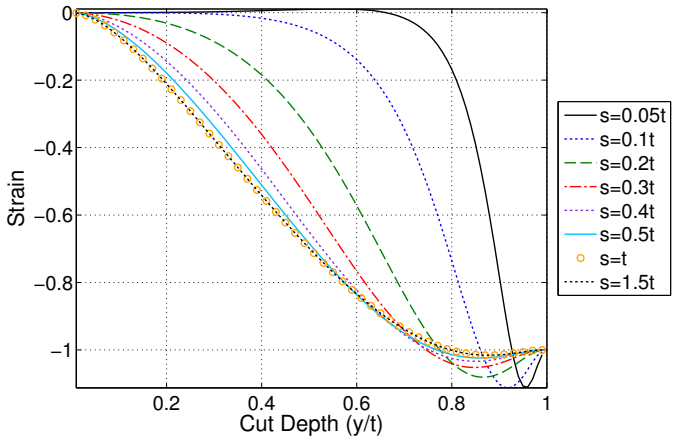

Fig. 14 – Strain versus cut depth for a second order Legendre stress (i.e. one column of the compliance matrix) and different values of s

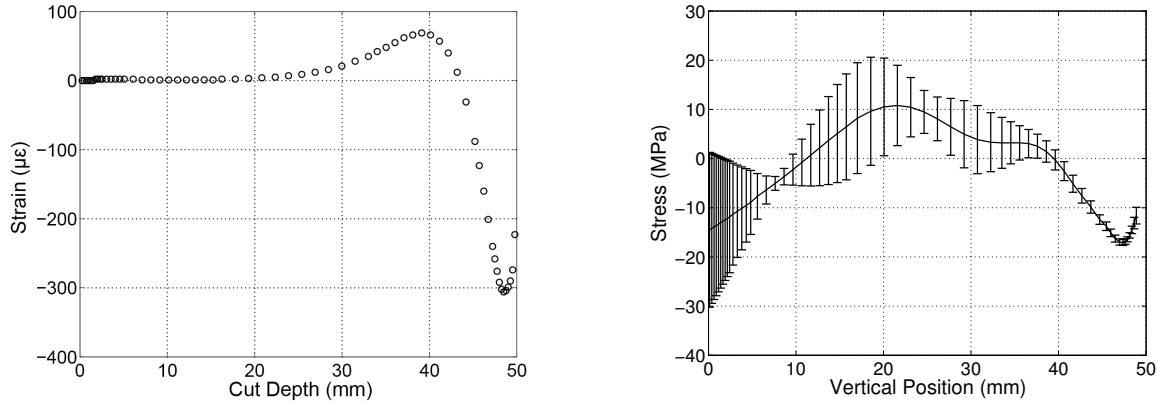

(a) (b)

Fig. 15 – Slice 4, cut 2 at x = 0 (a) measured strain and (b) calculated stress with uncertainty

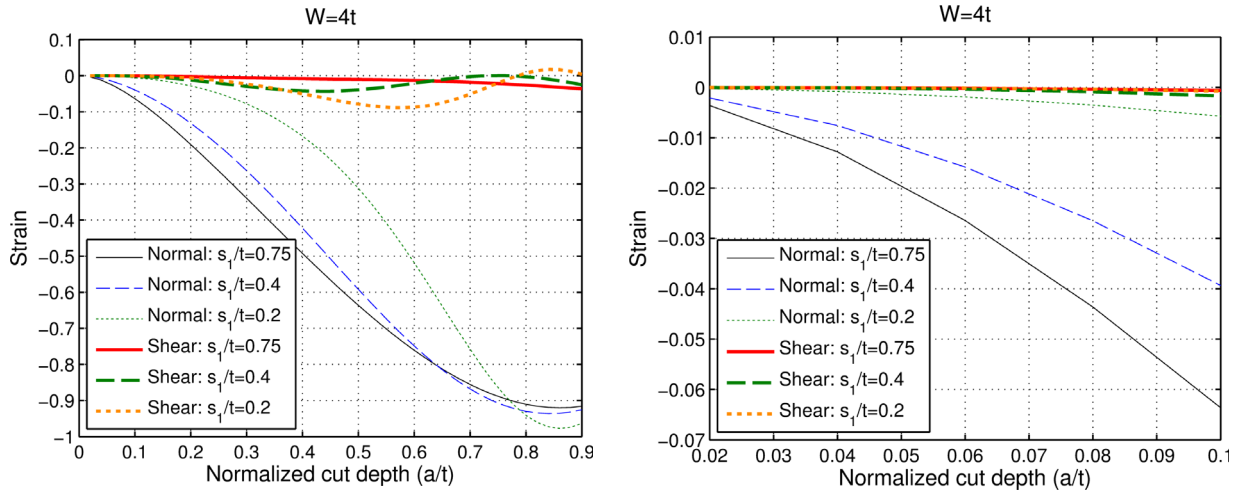

(a) (b)

Fig. 16 – Strain response for normal (L_2) and shear (modified J_1) tractions for $W_1 = 4t$ for (a) the full cut depth range and (b) initial cut depths

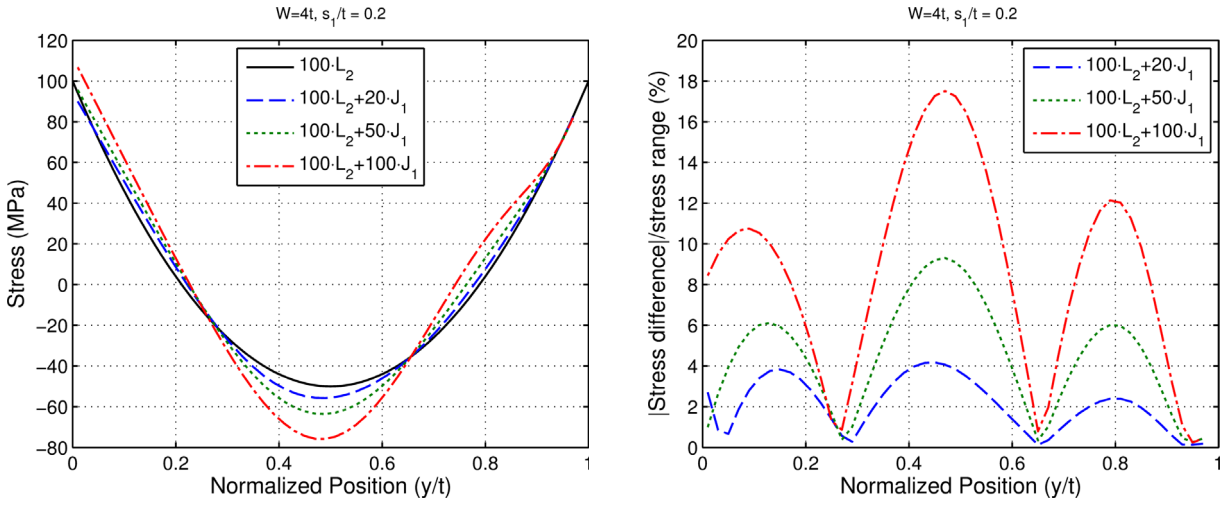

Fig. 17 – (a) Computed slitting stress with a normal stress of $100L_2$ and various modified J_1 shear stresses and (b) percentage stress difference from $100L_2$ for $s_1 = 0.2t$ for $W_1 = 4t$

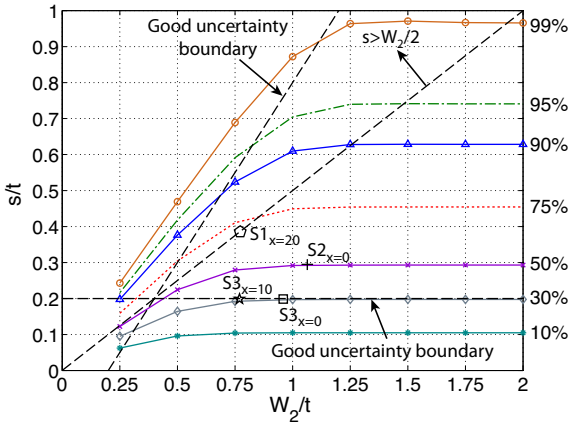

Fig. 18 – Plot of percentage of the maximum stress relative to the original present at a given lateral position (s/t) away from a previous slitting measurement plane as a function of specimen width (W_2/t) for samples with variable width with the position from the cut plane normalized by t. Dashed lines indicate boundaries for good uncertainty (horizontal line for s/t = 0.2 and angled line for spacing from far edge equal to 0.2t). The physical experiment in slice 3, cut 2 at x = 0 is shown with a square marker, slice 3, cut 3 at x = 10 mm is shown with a star marker, slice 1, cut 3 at x = 20 mm is shown with a pentagon marker, and slice 2, cut 2 at x = 0 is shown with a plus marker

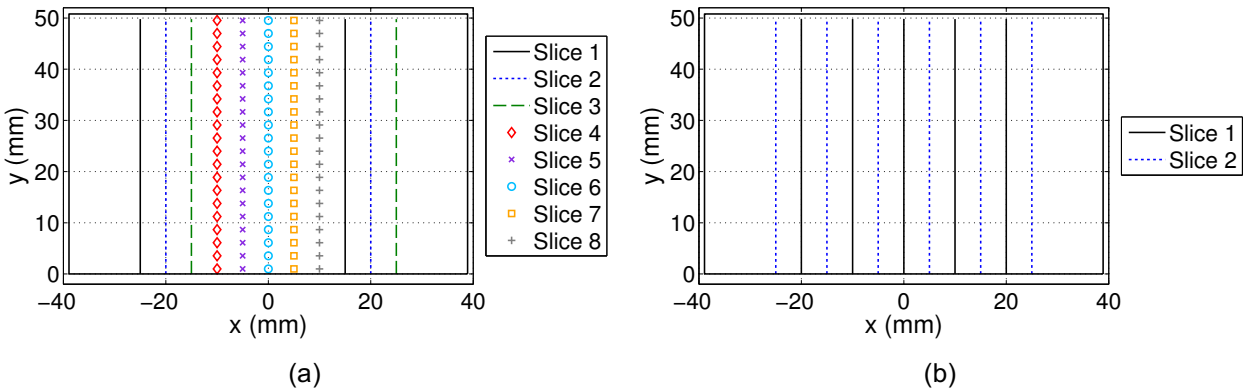

Fig. 19 – (a) Measurement locations with no corrections needed between measurements (uses 8 slices) and (b) with minimum recommended spacing between measurements (uses 2 slices)

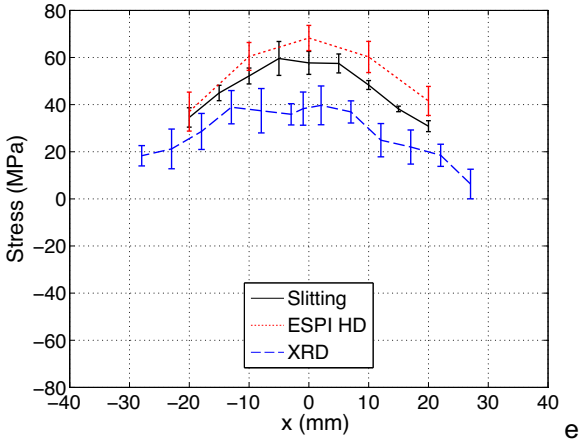

Fig. 20 – Line plot showing the stress measured at y = 25.4 mm from slitting, ESPI hole drilling (HD), and x-ray diffraction (XRD)